



## OPEN ACCESS

## EDITED BY

Lian Xiang Luo,  
Guangdong Medical University, China

## REVIEWED BY

Junke Wang,  
University of Texas MD Anderson  
Cancer Center, United States  
Hua Zhong,  
University of Hawaii at Manoa,  
United States

## \*CORRESPONDENCE

Senling Feng  
2019683088@gzhmu.edu.cn  
Wenfei Zhong  
928954146@qq.com

<sup>†</sup>These authors have contributed  
equally to this work

## SPECIALTY SECTION

This article was submitted to  
Pharmacology of Anti-Cancer Drugs,  
a section of the journal  
Frontiers in Oncology

RECEIVED 31 August 2022

ACCEPTED 27 September 2022

PUBLISHED 17 October 2022

## CITATION

Huang H, Dai Y, Duan Y, Yuan Z, Li Y,  
Zhang M, Zhu W, Yu H, Zhong W and  
Feng S (2022) Effective prediction of  
potential ferroptosis critical genes in  
clinical colorectal cancer.  
*Front. Oncol.* 12:1033044.  
doi: 10.3389/fonc.2022.1033044

## COPYRIGHT

© 2022 Huang, Dai, Duan, Yuan, Li,  
Zhang, Zhu, Yu, Zhong and Feng. This is  
an open-access article distributed under  
the terms of the [Creative Commons  
Attribution License \(CC BY\)](https://creativecommons.org/licenses/by/4.0/). The use,  
distribution or reproduction in other  
forums is permitted, provided the  
original author(s) and the copyright  
owner(s) are credited and that the  
original publication in this journal is  
cited, in accordance with accepted  
academic practice. No use,  
distribution or reproduction is  
permitted which does not comply with  
these terms.

# Effective prediction of potential ferroptosis critical genes in clinical colorectal cancer

Hongliang Huang<sup>1,2,3†</sup>, Yuexiang Dai<sup>4†</sup>, Yingying Duan<sup>1,2,3†</sup>,  
Zhongwen Yuan<sup>1,2,3</sup>, Yanxuan Li<sup>5</sup>, Maomao Zhang<sup>5</sup>,  
Wenting Zhu<sup>1,2</sup>, Hang Yu<sup>1,2</sup>, Wenfei Zhong<sup>1,2\*</sup>  
and Senling Feng<sup>1,2,3\*</sup>

<sup>1</sup>Department of Pharmacy, The Third Affiliated Hospital of Guangzhou Medical University, Guangzhou, China, <sup>2</sup>Guangdong Provincial Key Laboratory of Major Obstetric Diseases, Guangzhou, China, <sup>3</sup>School of Pharmaceutical Sciences, Guangzhou Medical University, Guangzhou, China, <sup>4</sup>School of Pharmacy, Guangdong Pharmaceutical University, Guangzhou, China, <sup>5</sup>The Fifth Affiliated Hospital of Guangzhou Medical University, Guangzhou, China

**Background:** Colon cancer is common worldwide, with high morbidity and poor prognosis. Ferroptosis is a novel form of cell death driven by the accumulation of iron-dependent lipid peroxides, which differs from other programmed cell death mechanisms. Programmed cell death is a cancer hallmark, and ferroptosis is known to participate in various cancers, including colon cancer. Novel ferroptosis markers and targeted colon cancer therapies are urgently needed. To this end, we performed a preliminary exploration of ferroptosis-related genes in colon cancer to enable new treatment strategies.

**Methods:** Ferroptosis-related genes in colon cancer were obtained by data mining and screening for differentially expressed genes (DEGs) using bioinformatics analysis tools. We normalized the data across four independent datasets and a ferroptosis-specific database. Identified genes were validated by immunohistochemical analysis of pathological and healthy clinical samples.

**Results:** We identified DEGs in colon cancer that are involved in ferroptosis. Among these, five core genes were found: *ELAVL1*, *GPX2*, *EPAS1*, *SLC7A5*, and *HMGB1*. Bioinformatics analyses revealed that the expression of all five genes, except for *EPAS1*, was higher in tumor tissues than in healthy tissues.

**Conclusions:** The preliminary exploration of the five core genes revealed that they are differentially expressed in colon cancer, playing an essential role in ferroptosis. This study provides a foundation for subsequent research on ferroptosis in colon cancer.

## KEYWORDS

bioinformatics, colon cancer, ferroptosis, differentially expressed genes, data mining, lipid peroxidation

## Introduction

Colon cancer is one of the most common and aggressive cancers worldwide, with high morbidity and poor prognosis. It is considered one of the most severe cancers, along with lung, prostate, and breast cancers (1). Up to 20% of colon cancers may be determined by genetic alterations and are primarily inherited diseases caused by overexpression of oncogenes and inactivation of tumor suppressor genes. Therefore, colon cancer is also influenced by several factors, including age and diet (2). This is because dietary factors can contribute to genetic changes or regulate other processes in cancer development. For instance, meat and fat seemingly increase the formation of free radicals in the intestine, primarily reactive oxygen species (ROS) (3). Free radicals, including oxygen radicals and lipid degradation products (i.e., 4-hydroxyalkenes and aldehydes), are genotoxic (4). Colon cancer is associated with reduced immune cytotoxicity (5) and diminished T-cell infiltration (6). Treatment for this cancer includes traditional surgery, radiotherapy, and chemotherapy, as well as risk factor modification, screening prevention, early diagnosis, and rapidly evolving immunotherapy (7). Adjuvant therapy may provide a survival advantage for some patients with colon cancer (e.g., stage III or II). However, not all patients benefit from these treatments (8). Therefore, it is necessary and urgent to explore new biomarkers and molecular mechanisms for targeted therapy of colon cancer to significantly improve patient prognosis and reverse cancer drug resistance.

Cell death is a fundamental physiological process for cell development, aging, and tissue homeostasis, which are hallmarks of cancer. Ferroptosis, a novel term created in 2012 by Dr. Brent R. Stockwell, describes a non-apoptotic form of programmed cell death dependent on intracellular iron (9). It is morphologically and biochemically distinct from other types of cell death and is characterized by an iron-dependent mechanism of intracellular lipid peroxidation induced by ROS. Ferroptosis is an essential cell death pathway that plays a crucial role in various diseases, including cancer, cardiovascular, and neurological diseases. In some cases, tumor metabolic reprogramming is associated with sensitivity to ferroptosis (10–12). Thus, a better understanding of the mechanisms underlying ferroptosis and the consequent development of new therapeutic strategies for treating tumor drug resistance would favor human health.

Bioinformatics and other computational tools, including artificial intelligence, play critical roles in medical care (13). We used a bioinformatics approach to preliminarily explore essential genes with a role in ferroptosis in colon carcinogenesis. We applied data mining and data analysis techniques to screen for differentially expressed genes (DEGs) in pathological and healthy tissues of patients with colon cancer. These DEGs were then intersected with ferroptosis-related genes from the ferroptosis-specific database yielding critical genes

associated with ferroptosis in colon cancer using various bioinformatics methods. In addition, we selected clinical tissue samples to validate these genes by immunohistochemistry. Our results contribute to the preliminary understanding and exploration of key genes that regulate ferroptosis in colon cancer, providing new ideas for targeted clinical therapy.

## Materials and methods

### Colon cancer-related gene expression and clinical data collection and processing

Gene expression profiles and related clinical data were obtained from a public database. Gene Expression Omnibus (GEO; <https://www.ncbi.nlm.nih.gov/geo/>), a gene expression database established by the National Center for Biotechnology Information (NCBI), contains gene expression data, including gene chips and high-throughput sequencing data. The microarray expression datasets, GSE41328, GSE44076, GSE110223, and GSE110225, were downloaded from the GEO database, and DEGs were accessed by comparing healthy colon tissue with colon cancer tissue (14). Dataset GSE41328 enclosed five colorectal adenocarcinomas and matched healthy colon tissues analyzed using the GPL570 array platform and Affymetrix HG-U133-Plus-2.0 microarrays. Dataset GSE44076 was acquired using Affymetrix Human Genome U219 Arrays on the GPL13667 platform to obtain gene expression profiles of paired healthy adjacent mucosal and tumor samples from 98 patients and 50 healthy individuals. GSE110223 and GSE110225 datasets contained DEGs of tumors and healthy colon tissue specimens, obtained by extracting total RNA using the GPL96 platform and further processing on the Affymetrix microarray platform HG-U133A.

All datasets were independent of each other and underwent the same processing. First, we download series matrix file(s) in the TXT format from each dataset to obtain the expression profile. To merge multiple data sets, we first merged the datasets using the R package *inSilicoMerging*, eliminating batch effects with the COMBAT method. Subsequently, we  $\log_2$ -transformed the data using the R package *limma* (version 3.40.6), a differential expression screening method based on generalized linear models, utilizing the *lmFit* function for linear regression. We further applied the *eBays* function for computing moderated t-statistics, moderated F-statistic, and log-odds of differential expression by empirical Bayes moderation of the standard errors. Finally, we obtained the DEGs between different pathological groups and control groups and plotted the differential gene volcanoes and sample clustering diagrams. Due to the excessive size of the feature matrix, we used principal component analysis (PCA) for dimensionality

reduction of the data using the R software (version). The R package *stats* (version 3.6.0) was applied to obtain the Z-score, and the *prcomp* function was used to reduce the dimensionality, yielding a reduced matrix that simplifies the analysis of each dataset, removes redundant features, reduces the number of characteristic attributes, and highlights the characteristic attributes under research.

## Ferroptosis and colon cancer co-regulated genes

Ferroptosis is a form of cell death that is morphologically and biochemically distinguished from apoptosis, classical necrosis, autophagy, and other forms of cell death. However, it also causes a decrease in cell number (15). Ferroptosis-related genes were identified by searching the keyword *ferroptosis* in the FerrDb database [<http://www.zhounan.org/ferrdb>; (16)], the first database containing regulators and markers of disease-associated ferroptosis. To identify co-regulated genes between the colon cancer-related DEGs and ferroptosis-related genes, all processed datasets were analyzed using the Venny 2.1.0 online software (<https://bioinfogp.cnb.csic.es/tools/venny/index.html>). The enriched pathways for these common genes were analyzed using Metascape [<http://metascape.org>; (17)] and WebGestalt [<http://www.webgestalt.org>; (18)] and visualized using the *ggplot2R* package.

## Colon cancer and ferroptosis biological networks

Weighted correlation network analysis (WGCNA) is a systems biology method that describes genetic associations between samples and can be applied to identify highly synergistic sets of genes and biomarker genes or therapeutic targets. It is based on the endogeneity of the gene set and the association between the gene set and phenotype. Therefore, we performed WGCNA to identify common biological networks between colon cancer and ferroptosis. First, we calculated the median absolute deviation (MAD) of each co-regulated gene found using the methodology described in Section 2.2 through their expression profiles. Subsequently, we eliminated the top 50% of the smallest genes, removing the genes and samples with zero variation using the *goodSamplesGenes* function using the R package. Next, the WGCNA package was also used to construct a scale-free co-expression network. Pearson's correlation matrixes and average linkage method were performed for all pairwise genes. A weighted adjacency matrix was constructed using the power function  $A_{mn} = |C_{mn}|^\beta$ , where  $A_{mn}$  is the adjacency between gene  $m$  and gene  $n$ ;  $C_{mn}$  is the Pearson's correlation between gene <sub>$m$</sub>  and gene <sub>$n$</sub> ;  $\beta$  is a soft-thresholding parameter that can emphasize the strong

correlations between genes. After a power of 18, the adjacency was transformed into a topological overlap matrix (TOM), a network gene pairing with the sum of the adjacencies of all other genes. Using the TOM, we measured the connectivity of the gene network and the corresponding dissimilarity (1-TOM).

The network type is unsigned, implying that genes within a module are highly correlated in an undirected network. To classify genes with similar expression into gene modules, average linkage hierarchical clustering was performed based on the TOM dissimilarity, with a minimum gene dendrogram size (genome) of 30. To further analyze the modules, we calculated the module eigengenes dissimilarity by setting the sensitivity to 3, selected a cut-off line for the module dendrogram, and merged a number of modules. It is possible to perform module-phenotype correlation analysis for each module after clustering genes into modules, draw a module-phenotype correlation heat map, divide samples into normal and tumor phenotypes, analyze the correlation phenotypes of modules of different colors corresponding to different phenotypes and identify the module with the highest correlation with the phenotype of interest.

## Protein-protein interaction analyses

The co-regulated DEGs found in Section 2.2 were also analyzed for their protein-protein interactions (PPIs) with the aid of the STRING online platform [<https://cn.string-db.org>; (19)]. The STRING database contains experimentally identified and predicted PPIs. The integrated networks were downloaded in the TSV format and imported into the Cytoscape 3.8.2 software. Network analysis and filtering-based top 10 degree values were implemented using the plug-in *cytohubba* and network analyzer tools. The Cytoscape application MCODE was used for clustering analysis of the gene networks to plot critical modules. Significantly enriched pathways for each module gene were analyzed through the online tools Metascape and WebGestalt, retaining ferroptosis-associated modules. The top 10 genes with degree values were merged with genes in critical modules, and duplicated genes were removed. The Cytoscape application MCODE was used for clustering analysis of the gene networks to plot critical modules.

## Functional enrichment analyses

Pathway enrichment analyses were performed for the genes screened in the 2.3 and 2.4 sections. We used the Kyoto encyclopedia of genes and genomes (KEGG) application programming interface (API, <https://www.kegg.jp/kegg/rest/keggapi.html>) for the R package *org.Hs.eg.db* (version 3.1.0) to acquire the latest KEGG pathway and gene ontology (GO) annotations as reference. Genes enrichment analyses were performed using the R package *clusterProfiler* (version 3.14.3),

with a minimum gene set of 5 and a maximum of 5000, p-value < 0.05, and FDR < 0.1. The Benjamini-Hochberg correction was applied to the p-values.

## Correlation analysis of survival time

The TCGA database (<https://www.cancer.gov>) and GEPIA 2.0. was used to integrate 2, 5, 9, and 10 years of survival time, survival status, gene expression data of colon cancer, and clinical information (20). The gene expression data of intersecting genes screened in Section 2.2 were used. The TCGA portal (21) and LinkedOmics were used to fit the data and filter the potential ferroptosis-related genes in colon cancer, according to the p-value ranking obtained from survival analysis combined with prognostic significance.

## Identification of key genes in colon tumors and healthy tissues

Genes in colon cancer tumors and healthy tissues were analyzed and compared using R packages, the TCGA and GTEx databases, and the online tools LinkedOmics, TCGA portal, and Sangerbox (22). LinkedOmics is a publicly available portal that includes multi-omics data from all 32 TCGA cancer types and ten clinical proteomics tumor analysis consortium (CPTAC) cancer cohorts (23). Data from the GTEx and TCGA datasets were normalized using the scale function in the R software, removing samples with null expression values. Further gene expression analysis of the TCGA pan-cancer and GTEx normalized samples was performed using the Wilcoxon test within the TCGA portal. Furthermore, differences in the expression of critical genes in different tissue sites in colon cancer samples (N:245) were calculated using R software (version 4.1.2) and the LinkedOmics database. The Kruskal-Wallis test was used to evaluate the significance of the DEGs. Final data analyses were visualized using multi-group box plots. We also performed mutation correlation analysis for key genes. The mutation annotation format (MAF) is a text format TCGA applies to store mutation annotation information. The MAF files of the TCGA database were used to identify differences in mutation frequencies in each set of samples by the chi-square test. The maftool R package was used to draw the waterfall plots.

Subsequently, we downloaded the uniformly normalized pan-cancer dataset TCGA TARGET GTEx (PANCAN, N = 19131, G = 60499) from the UCSC database (<https://xenabrowser.net/>), for mutual validation. Samples with no expression values or less than three replicates were filtered out, and  $\log_2(x + 0.001)$ -transformed. We used R software (version 4.1.2) to calculate expression differences between healthy and pathological colon samples and applied a non-parametric test to evaluate the statistical significance. Split violin plots were plotted with the ggplot2 function. The significance of gene differential

expression levels in different tumor stages (COAD: Stage I = 66, Stage II = 63, Stage III = 61, Stage N = 206) were calculated using the unpaired Student's t-test; non-parametric tests were used to assess the statistical significance of differences between multiple samples. Graphs were drawn on the bioinformatics platform (<https://www.bioinformatics.com.cn>).

## Immune cells infiltration correlated with key genes in colon cancer

TIMER assesses the infiltration of six immune cell types (B cells, CD4<sup>+</sup> T cells, CD8<sup>+</sup> T cells, neutrophils, macrophages, and dendritic cells) using the TIMER algorithm (24). Based on this platform, the expression profiles of colon cancer-related genes obtained by the method described in Section 2.5 were mapped to Gene Symbol. Samples with expression levels of 0 were filtered out using the Timer method of the R package IOBR (version 0.99.9) (25). Each expression value was  $\log_2(x + 0.001)$ -transformed, and significant relationships between essential genes and immune cells were calculated. Spearman's correlation coefficient between core genes was calculated using the corr test function of the R package psych (version 2.1.6). The bioinformatics platform was used for data visualization.

## Immunohistochemical analysis of critical genes in colon samples

Colon tissue samples were obtained from the Third Affiliated Hospital of Guangzhou Medical University (Guangzhou, China). All samples were collected after obtaining informed consent from patients. The experiments were approved by the ethics committee of the Third Affiliated Hospital of Guangzhou Medical University (number: 2022-076).

All samples were oven baked at 70°C for 1 h. Next, xylene (I, II), absolute ethanol, 95% ethanol, and 75% ethanol were added in this order for dewaxing. Antigen repairing of tissue sections was performed to fully expose antigenic sites using 0.01 M citrate buffer in a 95°C water bath for 15 min, followed by natural cooling to room temperature. SP Rabbit & Mouse HRP kits (DAB) were purchased from CWBIO Co., Ltd. (Lot. 25121). Endogenous peroxidase blocking solution and standard sheep serum working solution were added and incubated at room temperature. Antibodies were diluted to the appropriate concentration and incubated overnight at 4°C. Biotin-labeled sheep anti-rabbit or mouse secondary antibodies, and HRP-labeled streptavidin were added dropwise and incubated at room temperature for 15 min. Next, DAB color development solution and hematoxylin were added dropwise. Films were sealed and stored after dehydration and air-drying and photographed under an inverted fluorescence microscope (Nikon ECLIPSE Ti2). The design diagram in this paper is shown in Figure 1 for reference.

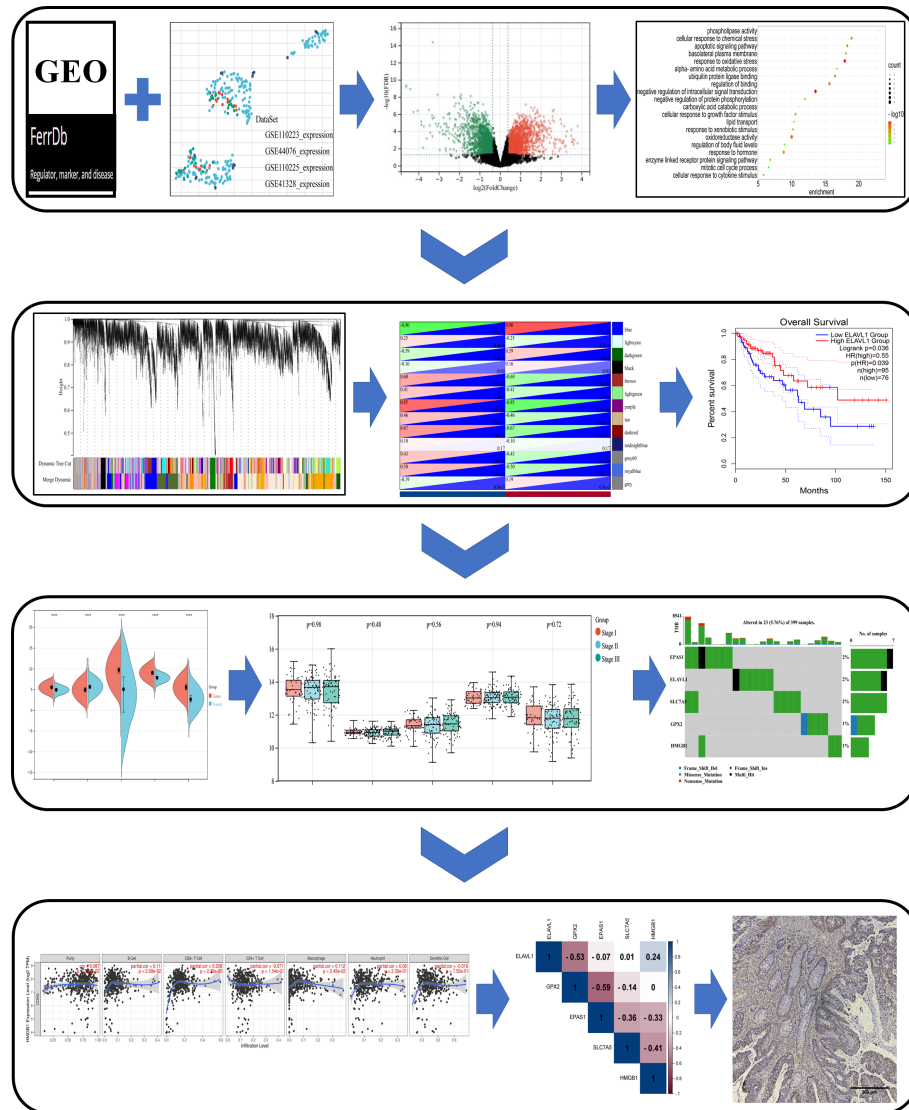


**FIGURE 1** Schematic diagram of the study design. Differentially expressed genes (DEGs) associated with ferroptosis were identified in the GEO dataset and FerrDb database. Based on these DEGs, a study was conducted in the Metascape, WebGestalt database for enrichment analysis, and WGCNA and PPI analysis, and were analyzed by Cox survival analysis to obtain the key genes. The core genes were evaluated in multiple databases for gene characterization, downstream functional enrichment, mutational analysis and immune cell infiltration associated with ferroptosis. Validation of core gene expression by clinical samples from colon cancer patients.

## Results

### Colon cancer alters genes expression profiles relative to healthy tissue

As shown in the box plots and density plots, the sample distributions of each dataset differed significantly. In addition, the UMAP plots showed that samples of each dataset clustered together individually, suggesting a batch effect (Supplementary Figure 1). After eliminating the batch effect, given the size of the

dataset, we performed the same analysis on each dataset individually and finally merged the results. DGEs between healthy and colon cancer samples with more than 1.3-fold change ( $\log_{2}FC > 0.3$ ) and  $p$ -value  $< 0.05$  obtained from all databases and analysis are shown in Figures 2A–D and Table 1 (26). The clustering results revealed two main clusters (Supplementary Figure 2). PCA facilitates the observation and mining of information from healthy vs. pathological tissue samples and visualizes the characteristics of both sets. As displayed in Figures 2E–H, the scatter points corresponding to

the samples of the four groups overwhelmingly converged, indicating that the repetition between groups was relatively good and sample data were similar. Notably, the volcano plot in [Figure 2E](#) did not overlap, suggesting that the samples were well differentiated. Although samples illustrated in [Figures 2F–H](#) overlapped to some extent, the overlap was not significant, and the samples were not substantially similar. In summary, we hypothesize that colon cancer alters the gene expression profiles compared to healthy colon tissue.

## DEGs are engaged in biological processes and signaling pathways associated with ferroptosis

In the FerrDb database, 259 ferroptosis genes were retrieved, including drivers (108), suppressors (69), and markers (111), among which 28 were annotated with multiple functions. There were 79, 37, 211, and 234 co-regulated genes between ferroptosis and colon cancer datasets ([Figures 3E–H](#)). The enrichment analysis revealed that the ferroptosis-related DEGs were enriched in biological processes, such as cellular response to chemical stress, antioxidant activity, cellular response to metal ions, ROS metabolic process, response to oxidative stress, oxidoreductase activity, response to oxygen levels, positive regulation of cell death, and response to iron ions ([Figures 3A–D](#)). KEGG functional analysis revealed that signaling pathways, such as ferroptosis, p53, mTOR, PPAR, and HIF-1 signaling pathways, were significantly activated in colon cancer tissues ([Figures 3E–H](#)). Notably, the ferroptosis pathway is the main pathway involved, as confirmed by Metascape and WebGestalt. Therefore, DEGs are involved in biological processes and signaling pathways related to ferroptosis.

## Modular genes constructed by WGCNA might play an essential role in colon carcinogenesis

An essential process in the construction of a WGCNA is the selection of soft-thresholding power. GSE41328, GSE44076, GSE110223, and GSE110225 were identified to have soft thresholds of 18, 10, 9, and 18, respectively. The lowest power relative balanced scalar independence of the scale-free topological fit indices was 0.86, 0.85, 0.85, 0.85, and the average connectivities were 21.40, 56.60, 18.76, and 5.62 for the datasets GSE41328, GSE44076, GSE110223, and GSE110225, respectively ([Supplementary Figure 3](#)). This suggests high independence and co-expression similarity of gene expression profiles between each module and within the modules.

Therefore, we merged modules with distances less than 0.25, resulting in modules for further WGCNA analysis, whereas gray modules were considered to be sets of genes that could not be assigned to any module ([Figures 4A–D](#)). GSE41328 obtained 28

modules, in which the antiquewhite2 module had 2275 genes, and the heat diagram was plotted according to the selected modules with clinical characteristics. The results showed that the modules strongly correlated with healthy colon tissue ([Figure 4E](#)). GSE44076 yielded 13 modules; the blue module had 3,404 genes, and the phenotype-associated heat map showed a high correlation between this module and colon cancer tissues ([Figure 4F](#)). Twenty-one modules were obtained for GSE110223, in which the pink module had 3,427 genes, and the module-phenotype correlation heat map showed a strong correlation between the module and colon cancer ([Figure 4G](#)). GSE110225 yielded 12 modules; the cyan module had 2634 genes, and a strong correlation was observed for the module-phenotype correlation heat map between this module and the occurrence of colon cancer ([Figure 4H](#)), indicating that the genes identified in the WGCNA analysis may play an important role in colon cancer.

## PPI network analysis revealed ferroptosis-related gene networks

Clustering analysis of the PPI networks of the GSE41328, GSE44076, GSE110223, and GSE110225 datasets yielded five, three, ten, and ten modules containing 59, 20, 632, and 643 genes, respectively ([Supplementary Figure 4](#)). The top 10 genes with degree values and module genes were merged, and duplicate values were removed, obtaining a total of 129 ferroptosis-related DEGs.

## Ferroptosis in colon cancer regulate a set of genes involved in the same pathway

A total of 25 genes co-regulated during ferroptosis and colon cancer were identified by PPI and WGCNA analysis ([Figure 5A](#)). GO enrichment analysis showed that these 25 co-regulated genes were significantly enriched in cellular response to chemical stress, antioxidant activity, response to metal ions, ROS metabolic process, and other biological processes associated with ferroptosis ([Figure 5B](#)). Furthermore, the 25 genes were significantly enriched for ferroptosis pathway, p53 signaling pathway, and glutathione metabolism, which included genes such as those encoding glutathione peroxidase 2 (*GPX2*), endothelial PAS domain protein 1 (*EPAS1*), solute carrier family 7 member 5 (*SLC7A5*), and mitogen-activated protein kinase 3 (*MAPK3*; [Figures 5C, D](#)). These genes are potential marker candidates for ferroptosis in colon cancer.

## Ferroptosis genes inhibit the development and progression of colon cancer

According to the colon cancer Cox regression test ([Table 2](#)) and Kaplan–Meier (K–M) curves of key genetic risk factors ([Figure 6](#)), the five most significant genes selected were:

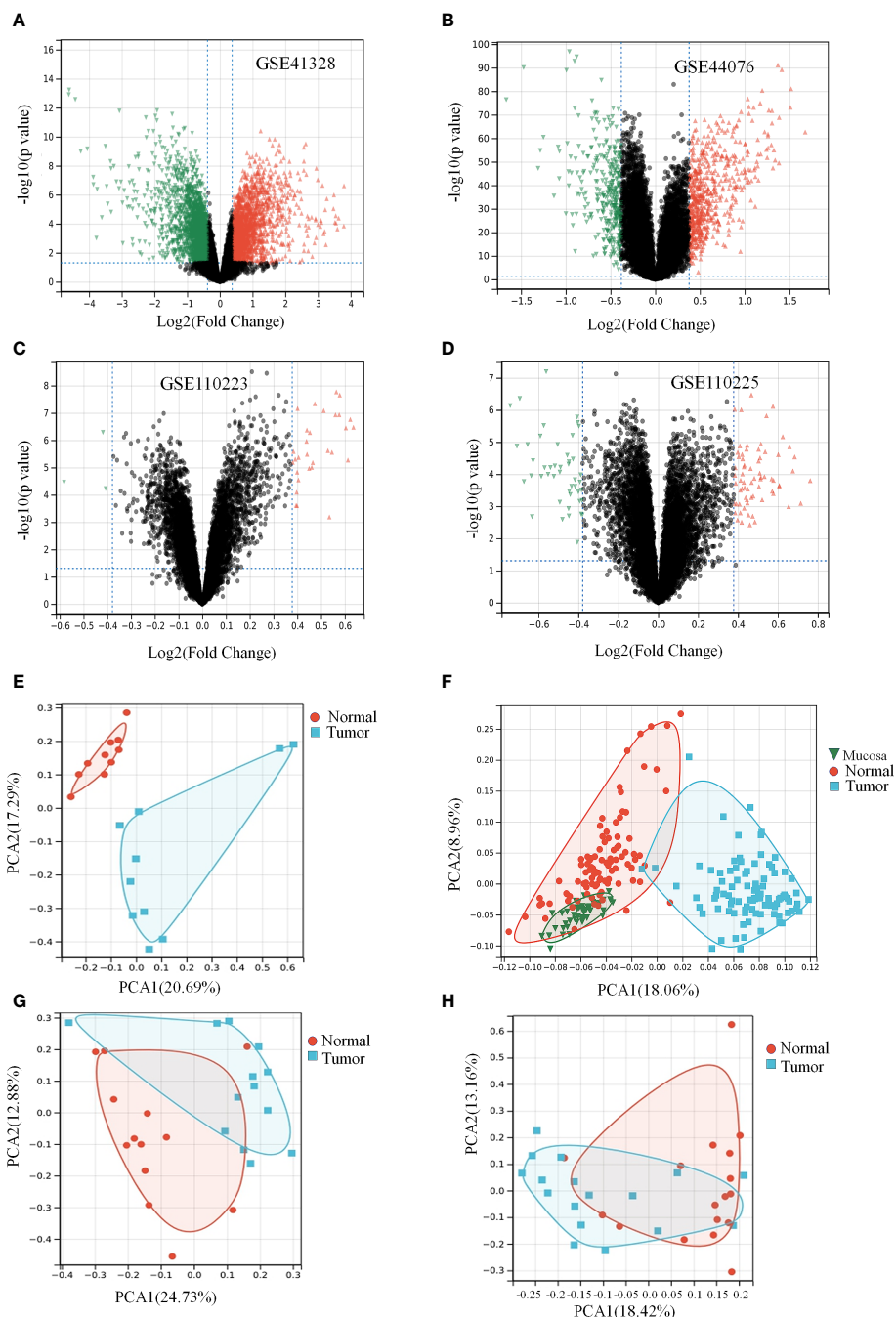


**FIGURE 2**  
 Colon cancer differentially causes the expression of genes in a certain extent. (Table 1) Expression differences of genes in data set. (A, E) Differential gene volcano plot and PCA analysis plot of GSE41328 dataset. (B, F) Differential gene volcano plot and PCA analysis plot of GSE44076 dataset. (C, G) Differential gene volcano plot and PCA analysis plot of GSE110223 dataset. (D, H) Differential gene volcano plot and PCA analysis plot of GSE110225 dataset.

ELAV-like RNA-binding protein 1 (*ELAVL1*), *GPX2*, *EPAS1*, *SLC7A5*, and high mobility group box 1 (*HMGB1*). A total of 399 samples with detected mutations were analyzed to correlate the mutations with these core genes, of which 23 (5.76%) were included in the mapping samples. We identified mainly missense

mutations, single nucleotide polymorphism (SNP), and single nucleotide variation (SNV) of C>T, in which *EPAS1* had the highest mutation frequency (Figures 7A, B).

The split violin plot diagram revealed that the expression profiles of these core genes in different databases of colon cancer

TABLE 1 Number of differentially expressed genes and background in the four data sets.

	GSE41328		GSE44076		GSE110223		GSE110225
sample number	20		246		26		34
platform	GPL570		GPL13667		GPL96		GPL96&GPL570
molecule	total RNA		total RNA		total RNA		total RNA
source	Normal, matched normal colon tissue		Healthy colon mucosa cells		normal adjacent sample		normal adjacent sample
	Tumor, colon adenocarcinoma		Normal distant colon mucosa cells Primary colon adenocarcinoma cells		primary colorectal adenocarcinoma		primary colorectal adenocarcinoma
Submission date	3-Oct-12		5-Feb-13		6-Feb-18		6-Feb-18
Last update date	25-Mar-19		31-Aug-21		6-Mar-19		25-Mar-19
Contact name	Chieh-Chun Chen		Victor Moreno		Aristotelis Chatziioannou		Aristotelis Chatziioannou
ZIP/Postal code	61801		8908		11635		11635
Country	USA		Spain		Greece		Greece
Number (1.3-fold change, significance threshold <0.05)	Up-regulation	Down-regulation	Up-regulation	Down-regulation	Up-regulation	Down-regulation	Down-regulation
	2319	2442	639	364	31	3	46

were higher in tumors than in healthy tissues, except for *EPAS1*, and the results were statistically significant (Figure 7C). The gene expression profiles in colon cancer were identified using TCGA and GTEx databases. Most tumor samples were distributed in stages I–III. However, bioinformatics analysis showed no statistically significant results in tumor stages (Figure 7D).

## Identification of ferroptosis-related genes by immune signature

The correlation between the five core genes and six immune cells was assessed using the TIMER platform. Expression of *ELAVL1* and *EPAS1* was positively correlated with all six immune cells analyzed, although a higher correlation was observed for CD4<sup>+</sup> T cells. Interestingly, all six immune cells negatively correlated with *GPX2*, which strongly correlated with neutrophils. *HMGB1* positively correlated with four immune cells except CD8<sup>+</sup> T. *SLC7A5* negatively correlated with CD8<sup>+</sup> T cells (Figures 8A, B).

The significant relationship of the core genes was analyzed, showing that *GPX2* was negative correlation with *EPAS1*; *ELAVL1* did not correlate with *GPX2*; *HMGB1* and *ELAVL1* were positively correlated, and *SLC7A5* was highly correlated with *ELAVL1* (Figure 8C and Supplementary Figure 6). IFN- $\gamma$  secreted by CD8<sup>+</sup> T cells can inhibit systemic *XC* expression, thus promoting iron-induced death in tumor cells (27). The infiltration of colorectal cancer (CRC) by CD8<sup>+</sup> T-expressing positive lymphocytes has been associated with a good prognosis (28).

## Immunohistochemical analysis

The results showed that the five core genes were expressed in stage I–III tumor tissues, as shown in Figure 9 and Supplementary Figure 5. According to the color and quantity of positivity: *ELAVL1* was expressed in stages I–III and was differentially expressed between tumor and normal tissues. The experimental results matched the results in Figure 7C. *EPAS1* was downregulated in tumor tissues relative to normal tissues, with significant differences between stages I and III, and II and III. The experimental results were consistent with the results shown in Figure 7C. *GPX2* was significantly upregulated in tumor tissues compared to normal tissues; there was no significant difference in stages I–III; experimental results validate the results shown in Figures 7C, D. *SLC7A5* was significantly upregulated in tumor tissues relative to normal tissues; experimental results validated the results shown in Figure 7C. *HMGB1* expression did not significantly differ between tumor and normal tissues. However, significant differences were observed between stages I and II and stages I and III. The experimental results were consistent with the results in Figure 7C.

## Discussion

Colon cancer is the third most common cancer worldwide and the leading cause of cancer-related death (29). Ferroptosis is a newly discovered form of regulated cell death governed by iron-dependent oxidative stress and lipid peroxidation (9, 30).

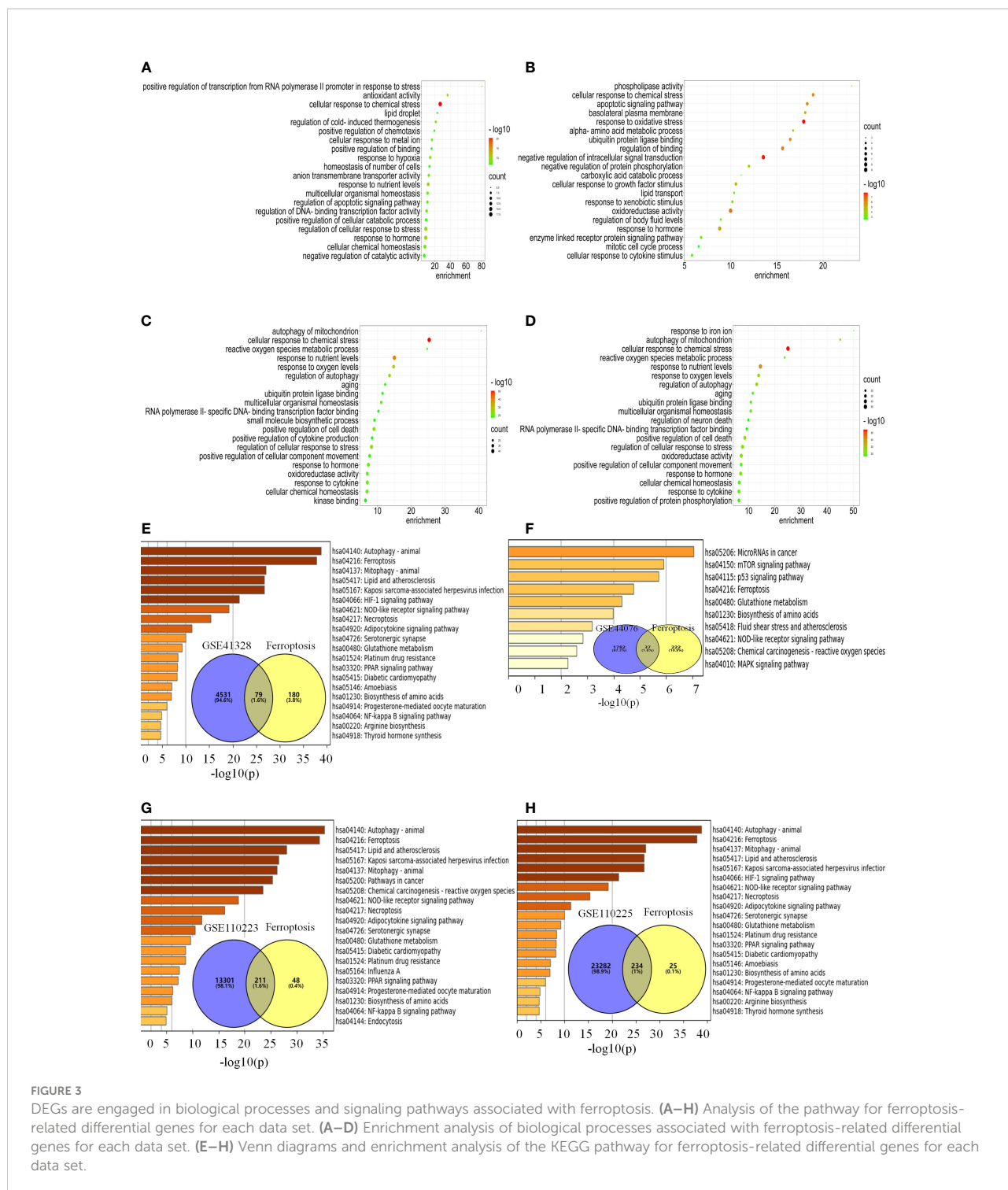
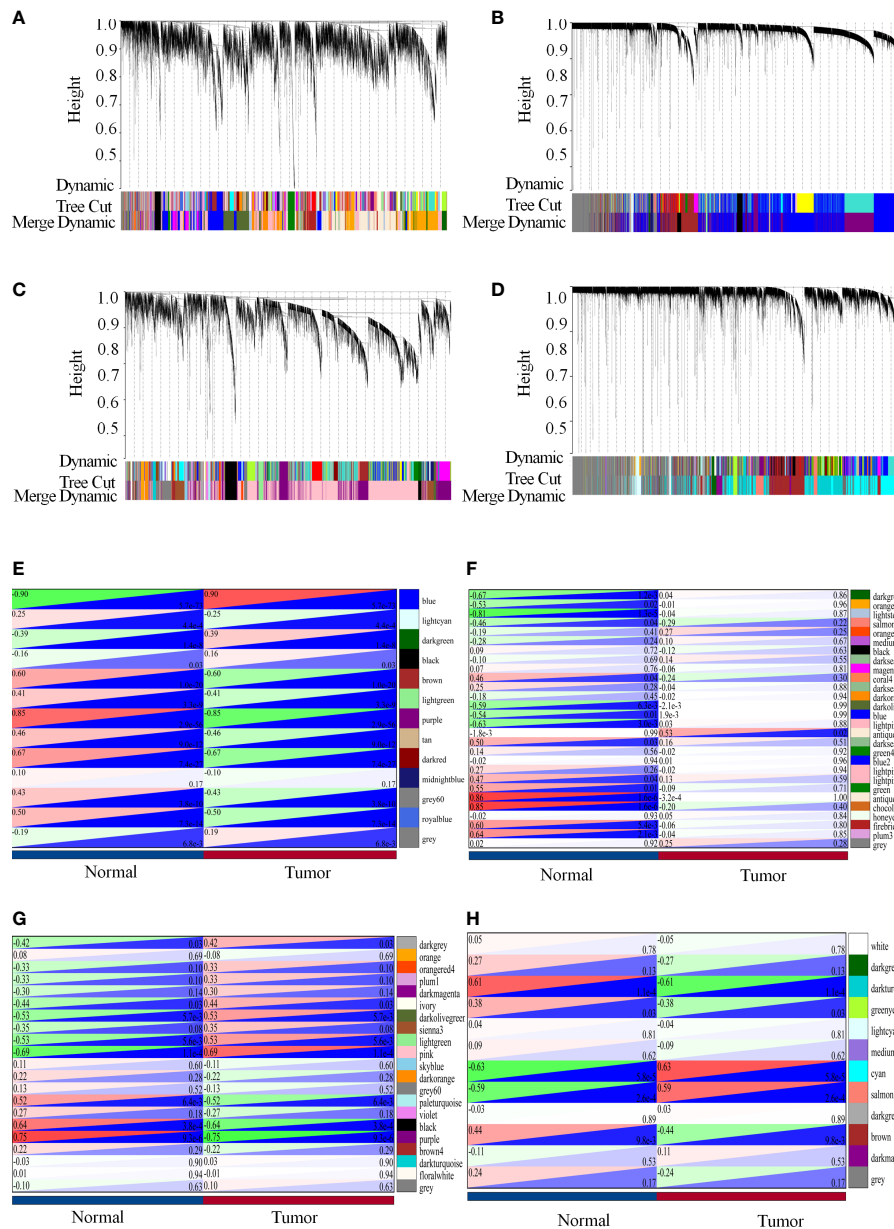


FIGURE 3

DEGs are engaged in biological processes and signaling pathways associated with ferroptosis. (A–H) Analysis of the pathway for ferroptosis-related differential genes for each data set. (A–D) Enrichment analysis of biological processes associated with ferroptosis-related differential genes for each data set. (E–H) Venn diagrams and enrichment analysis of the KEGG pathway for ferroptosis-related differential genes for each data set.

Iron, one of the most abundant transition metals in the body, plays a pivotal role in several biochemical reactions (31). Nevertheless, excessive iron is detrimental to cells, and ROS generated by lipid peroxidation, iron accumulation, and mediated by the Fenton reaction play a critical role in ferroptosis (32). Iron exists primarily in two oxidation states

in cells, ferrous ( $Fe^{2+}$ ) and ferric ( $Fe^{3+}$ ), which can accept and provide electrons. When overloaded with iron, catalytic  $Fe^{2+}$  is produced, causing a Fenton reaction that can convert hydrogen peroxide into toxic hydroxyl radicals ( $\cdot OH$ ). These free radicals attack lipids in the vicinity of membrane phospholipids. They can lead to polyunsaturated fatty acid (PUFAs) peroxidation and



**FIGURE 4**  
 Modular genes constructed by WGCNA possibly play an essential role in colon carcinogenesis. **(A–H)** WGCNA analysis of each data set. **(A, E)** WGCNA analysis of the GSE41328 dataset. **(A)** Co-expression modules of the GSE41328 dataset; **(E)** Relationship between selected modules and clinical features. **(B, F)** WGCNA analysis of the GSE44076 dataset. **(B)** Co-expression modules of the GSE44076 dataset; **(F)** Relationship between selected modules and clinical features. **(C, G)** WGCNA analysis of the GSE110223 dataset. **(C)** Co-expression modules of the GSE110223 dataset; **(G)** Relationship of selected modules to clinical features. **(D, H)** WGCNA analysis of the GSE110225 dataset. **(D)** Co-expression modules of the GSE110225 dataset, and heat maps based on adjacency relationships. **(H)** Relationship of selected modules with clinical features.

subsequent excessive ROS production, leading to DNA and protein damage and cellular ferroptosis (33, 34). Accordingly, ferroptosis is a novel, regulated form of cellular necrosis caused by excessive accumulation of ferrous iron and ROS (35).

In this study, we analyzed four datasets from public databases to identify DEGs between healthy and colon cancer

tissues. We performed co-regulation, WGCNA, and PPI analyses with ferroptosis-related genes from the FerrDb database using bioinformatics. We identified five core genes, *ELAVL1*, *GPX2*, *EPAS1*, *SLC7A5*, and *HMGB1*, involved in the ferroptosis of colon cancer. The expression of these genes was shown to be altered in the colon during carcinogenesis and

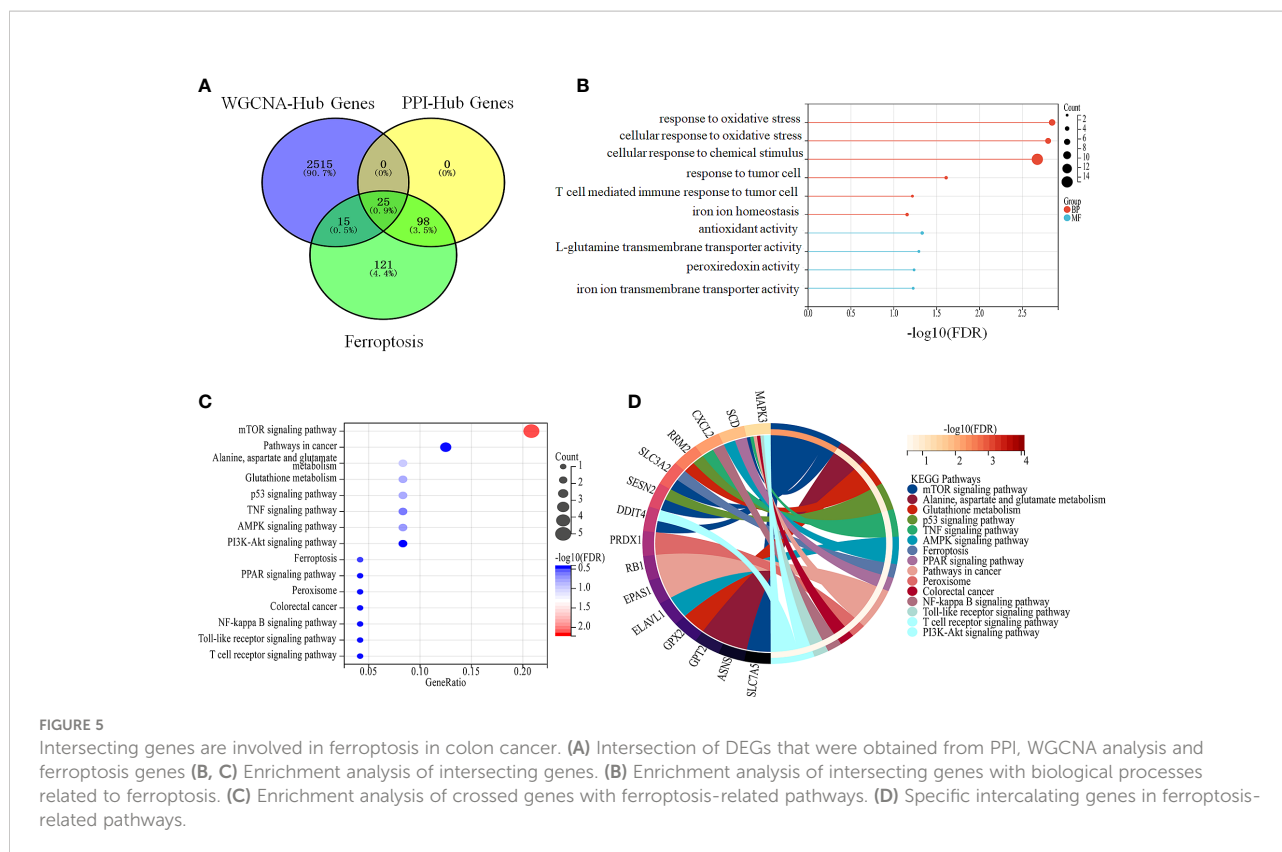


FIGURE 5

Intersecting genes are involved in ferroptosis in colon cancer. (A) Intersection of DEGs that were obtained from PPI, WGCNA analysis and ferroptosis genes (B, C) Enrichment analysis of intersecting genes. (B) Enrichment analysis of intersecting genes with biological processes related to ferroptosis. (C) Enrichment analysis of crossed genes with ferroptosis-related pathways. (D) Specific intercalating genes in ferroptosis-related pathways.

correlated with ferroptosis-related biological processes and signaling pathways. Moreover, according to *in silico* analysis and tissues immunohistochemical analysis, all genes except for EPAS1 were overexpressed in tumor tissues relative to healthy tissues.

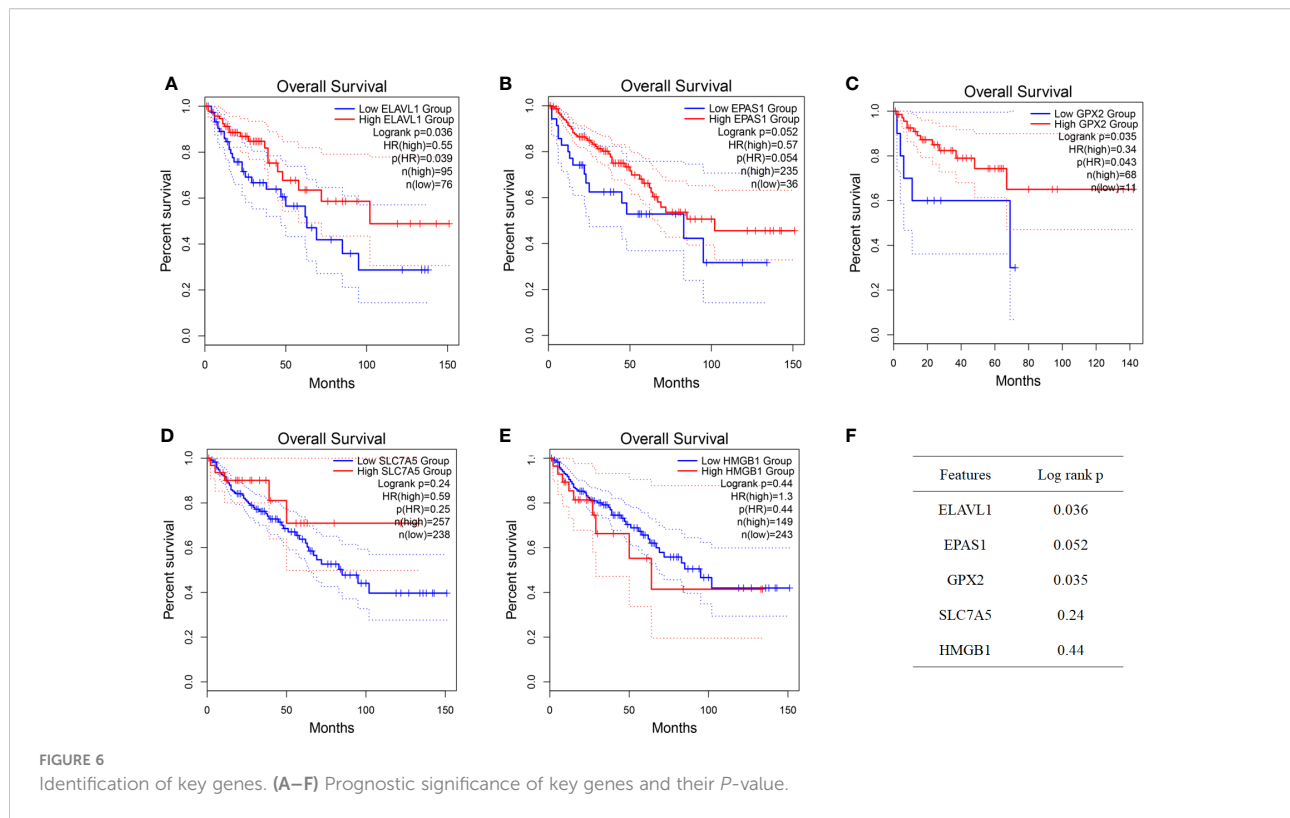
The messenger ELAVL1 is a cancer-associated RNA-binding protein, also known as human antigen R. It is a ubiquitous

TABLE 2 Name and P-value ranking of the 25 genes that intersect with PPI, WGCNA and ferroptosis genes.

Gene name	p-value	Gene name	p-value
ELAVL1	9.93E-01	ASNS	4.47E-01
GPT2	9.69E-01	GDF15	4.16E-01
MAPK3	9.27E-01	AURKA	3.70E-01
DDIT4	8.57E-01	SLC3A2	3.57E-01
GPX2	8.33E-01	SLC1A4	3.46E-01
EPAS1	8.27E-01	RRM2	3.01E-01
TRIB3	7.74E-01	STMN1	2.07E-01
TFR2	7.33E-01	TXNIP	1.95E-01
SLC7A5	6.72E-01	SCD	1.47E-01
PSAT1	6.57E-01	WIP1	1.02E-01
HMGB1	6.03E-01	CXCL2	5.85E-02
RB1	5.89E-01	SESN2	5.18E-02
PRDX1	4.64E-01		

member of the RBP family and acts as a positive regulator of RNA stability by stabilizing the 3'-untranslated region of the AU-rich cis-acting element (Ares) of the mRNA (36, 37). ELAVL1 targets include proto-oncogenes, growth factors, and invasive factors; thus, it plays an essential role in cancer (38). ELAVL1 expression is higher in almost all cancer tissues than in healthy ones (39). Immunohistochemical analysis of paired tumor and healthy tissues revealed that ELAVL1 expression and cytoplasmic abundance positively correlated with tumor malignancy and advanced tumor stage, especially in colon cancer (40, 41). ELAVL1 plays a vital role in activating iron-phagocytic proteins and promoting ferroptosis (42), altering cellular responses to oxidative stress, proliferation, differentiation, and immune stimulation (43, 44). Exposure to ferroptosis inducers results in a significant increase in ELAVL1 protein expression by inhibiting the ubiquitin-proteasome pathway. Besides, ELAVL1 overexpression appears to augment the production of autophagic vesicles, a potential mechanism for ELAVL1-promoted ferroptosis. However, ELAVL1 downregulation through RNA interference (RNAi) results in ferroptosis resistance (45).

Hypoxia is a tumor microenvironment hallmark that contributes to tumorigenesis and drug resistance development, which help tumors evade cell death through multiple mechanisms (46). Hypoxia-inducible factor 2-alpha (HIF2α), encoded by the EPAS1 gene, is an oxygen-sensitive component of HIF1 (47).



EPAS1 plays a critical regulatory role in ROS production and lipid metabolism in various cells (48, 49). *EPAS1* expression leads to increased tumor growth and metastasis (50) and is significantly associated with the occurrence, development, and prognosis of colorectal cancer. In colorectal cancer, *EPAS1* expression was negatively correlated with tumor grades, and mRNA expression of *EPAS1* was significantly lower in primary colorectal cancer tissues than in healthy tissues and correlated with advanced pathological stages III and IV and poor patient survival (51, 52). Furthermore, HIF-2 $\alpha$  activation in colon cancer enhances oxidative cell death by increasing cellular iron levels (53). HIF-2 $\alpha$  is selectively enriched in an acyl-CoA synthetase long-chain family member 4 (ACSL4)-dependent manner by polyunsaturated lipids that are required for lipid peroxidation and subsequent ferroptosis (54), which is promoted by lipid oxidation, ROS accumulation, and ferritin deposition (55).

The isozymes glutathione peroxidase 1 (GPX1) and GPX2 are the main enzymes responsible for hydrogen peroxide reduction in intestinal epithelial cells (56). GPX2 is loosely bound to the cytosolic side of the outer mitochondrial membrane and the matrix side of the inner mitochondrial membrane (57). In yeast, GPX2 counteracts the production of harmful ROS in the presence of PUFA, such as ROS produced in the mitochondria (58). The primary transcription factor that induces *GPX2* is the nuclear factor erythroid 2-related factor 2 (NRF2) (59). The expression profile of *GPX2* observed here is also likely transcriptionally regulated by NRF2. GPX2 knockdown is followed by NRF2-induced upregulation of GPX2 and

cytochrome c oxidase 2 (COX2), revealing the suppression of inflammation-mediated cancer (60). In human colon cancer, lipid peroxidation is directly proportional to the cancer stage (61). Specific ROS, such as hydrogen peroxide, are secondary messengers in the tumor signaling pathway. GPX2 keeps intracellular hydrogen peroxide levels low, thus maintaining clone formation and tumor cell numbers (62). GPX2 was the first protein to be identified as a target of the Wnt pathway (63). In inflammation-triggered carcinogenesis, GPX2 and the Wnt pathway co-localize at the base of intestinal crypts and are induced by Wnt signaling. When the Wnt pathway is dysregulated, GPX2 may promote tumor growth (64, 65).

The DNA-binding protein HMGB1 is a ubiquitous transcriptional regulator in almost all eukaryotic cells and is highly conserved between species without sequence specificity (66, 67). The HMGB1 protein is localized in the nucleus and translocated to the cytoplasm or extracellular space when stimulated by cytokines, lipopolysaccharides, or hypoxia (68, 69). Significantly elevated HMGB1 protein levels in colon cancer tissues are associated with poor prognosis and the absence of extensive macrophage infiltration (70). Similarly, HMGB1 is released upon exposure to various ferroptosis inducers (71). The secreted HMGB1 induces the matrix metalloproteinase pathway and increases the invasiveness of cancer cells (72). Oxidative stress can be prevented by inhibiting ferroptosis through the NRF2/HO-1/HMGB1 axis (73). HMGB1 also regulates ferroptosis *via* the Ras-JNK/p38 pathway in leukemia (74).

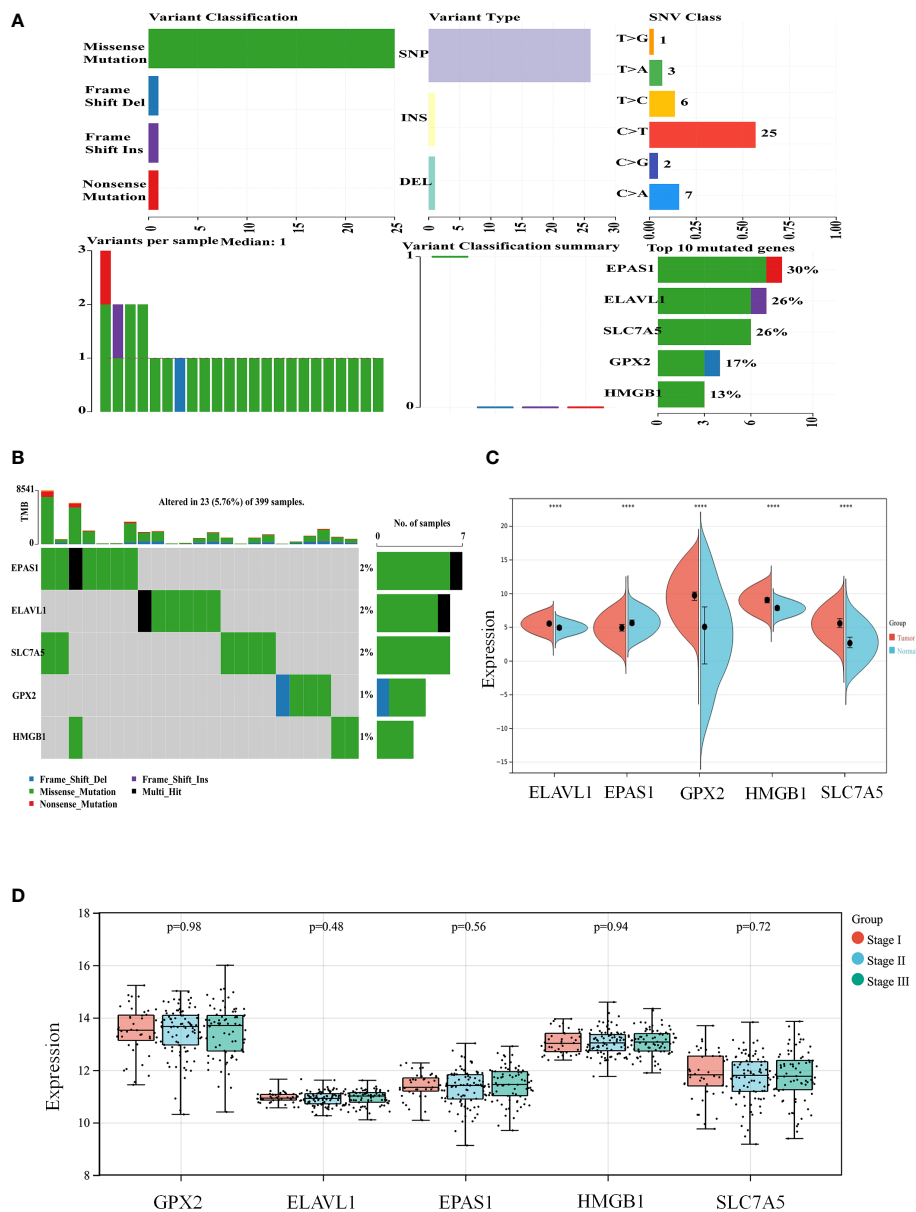


**FIGURE 7** The expression of key genes plays an important role in the development and progression of colon cancer. (A, B) Mutation correlation analysis of key genes. (C) Expression of the key genes in colon cancer tissues and in normal colon tissues from the UCSC database of colon cancer expression profiles. (D) Expression of key genes in different tumor stages. \*\*\*\* $P < 0.0001$ .

The human SLC7A5 transporter protein, also known as LAT1, is a sodium-independent reverse transporter positively regulated by physical interaction with membrane cholesterol and intracellular ATP, providing essential amino acids to the cell and maintaining dynamic cellular homeostasis (75, 76). SLC7A5 is overexpressed in the plasma membrane of aggressive cancer cells, and its expression level correlates with poor patient prognosis (77). In a pathological correlation study of non-small cell lung cancer (NSCLC) clinical stages I–III, the 5-year

survival rate of SLC7A5-positive patients was significantly lower than that of SLC7A5-negative patients (78). In addition, SLC7A5 is upregulated in cancer cells and exhibits high cancer specificity (79).

Our bioinformatics analysis showed no statistically significant results according to tumor stages. However, the expression of key genes was significantly different in tumor and normal tissues, as evidenced by statistical analysis of immunohistochemistry results, although the expression of

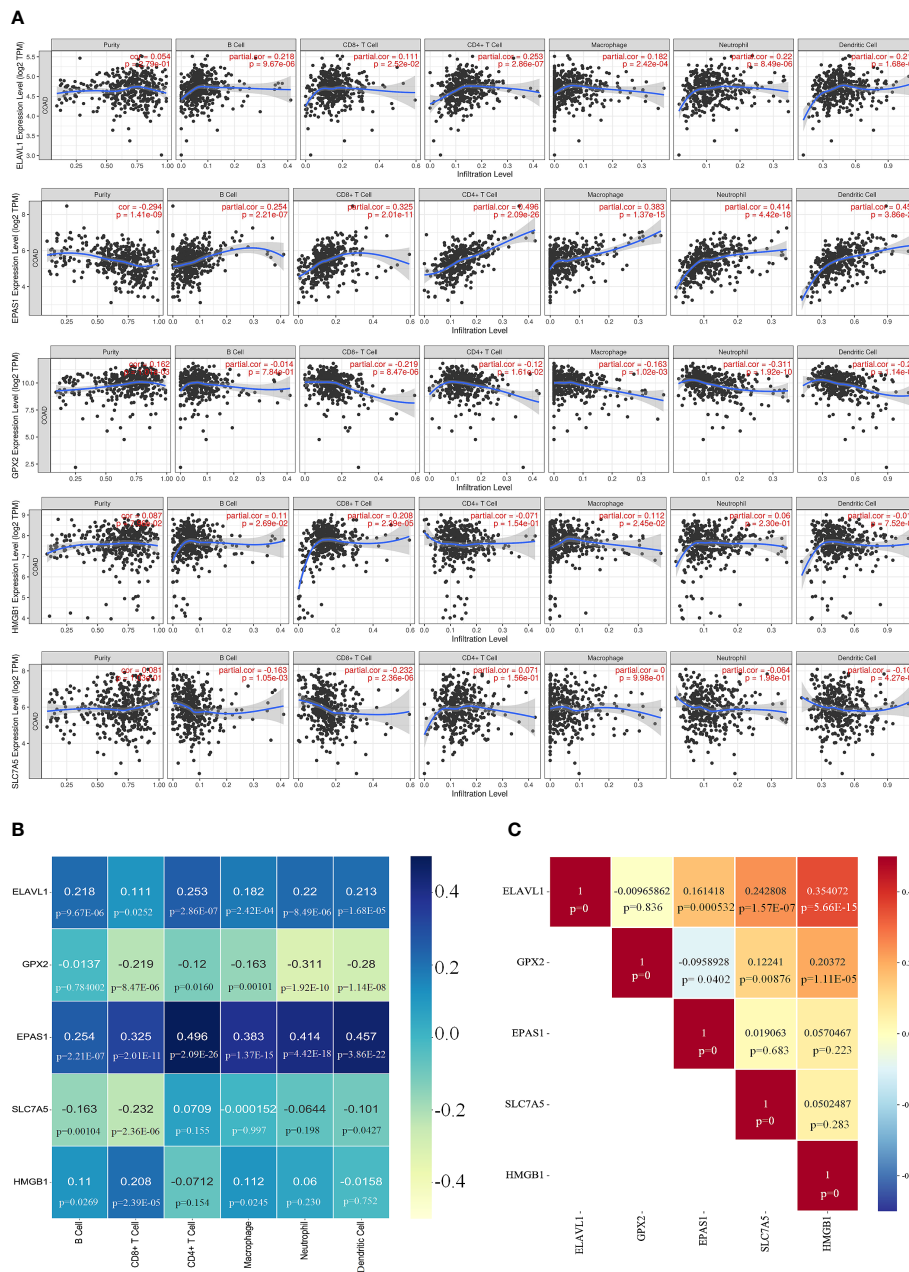


**FIGURE 8** Correlation of key genes and immune cells. (A, B) Correlation of five key genes with six immune cell. (C) Significant relationship between each core gene.

some genes did not significantly differ between tumor stages. Overall, the immunohistochemical experiments verified the bioinformatic predictions of core genes in normal and pathological tissues. Nonetheless, the results across tumor stages differed from the bioinformatic results. Possible reasons for the discrepancy might be the selection of data sets, differences in algorithms, datasets, databases, and clinical sample heterogeneity.

The currently available treatment strategies against colon cancer, a leading cause of cancer-related deaths worldwide, provide a survival advantage for some patients. However, not all patients benefit from these treatments. Therefore, novel biomarkers and molecular mechanisms must be identified to develop targeted colon cancer therapy, significantly improving the disease prognosis and reversing cancer drug resistance. Ferroptosis, a newly discovered form of iron-dependent cell death, could help

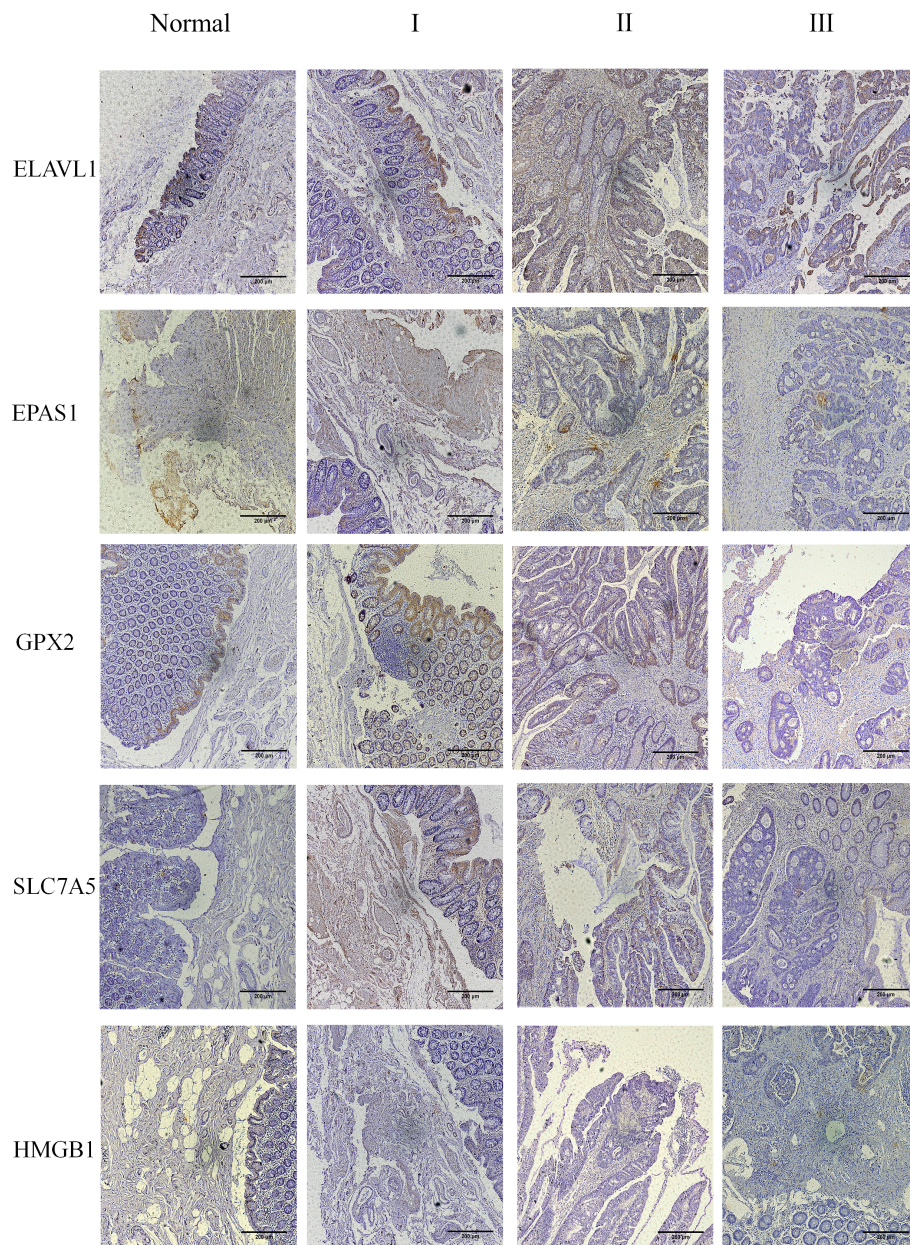


FIGURE 9

The five core genes were expressed in the tumor tissues of stage I–III. Clinical tissue samples were grouped in normal and tumor tissues (stage I–III), and the expression of the five key genes in the clinical samples was observed at multiples of 10X.

overcome tumor drug resistance and prevent cancer cell metastasis. To improve our understanding of the relationship between colon cancer and ferroptosis, we analyzed four datasets from public databases to identify DEGs between healthy and colon cancer tissues. We also performed co-regulation, WGCNA, and PPI analyses with ferroptosis-related genes from the FerrDb database. Our results suggest that five core genes, ELAVL1, GPX2, EPAS1, SLC7A5, and HMGB1, are involved in the ferroptosis of colon cancer cells. Finally, we validated the correlation of these genes with

colon cancer using immunohistochemical analysis of pathological and healthy clinical samples, confirming the different expression of all five genes in tumor tissues and healthy tissues were confirmed. We believe our study contributes significantly to the literature because our results open new possibilities in cancer therapy, providing new candidates for further studies on colon-targeted therapy and cancer drug resistance.

As a novel possibility in cancer therapy, ferroptosis inducers can help overcome tumor drug resistance, preventing metastasis

and the spread of cancer cells. Based on this, we initially explored key genes for ferroptosis in colon cancer and propose that the upregulation or downregulation of the five core genes identified here may be candidate targets for inducing ferroptosis in colon cancer cells. To further test this hypothesis, subsequent research on the ferroptosis pathways that involve these five genes in colon cancer is warranted. We believe this study provides a foundation for further research and new ideas for targeted therapy for colon tumors and cancer drug resistance.

## Data availability statement

The original contributions presented in the study are included in the article/[Supplementary Material](#). Further inquiries can be directed to the corresponding authors.

## Ethics statement

The studies involving human participants were reviewed and approved by Ethics Committee of the Third Affiliated Hospital of Guangzhou Medical University(number: 2022-076). The patients/participants provided their written informed consent to participate in this study.

## Author contributions

SF and WZ designed the research. HH, YDa and YDu carried out the experiments and performed data analysis. ZY, WZ, WZhu, YL, MZ and HY participated part of the experiments. HH, YDa and YDu wrote the manuscript. SF and WZ revised the manuscript. All authors contributed to the article and approved the submitted version.

## Funding

This work was supported by National Natural Science Foundation of China (No.82104446); Guangdong Basic and Applied Basic Research Foundation (No.2019A1515111109); Guangdong Province Characteristic Innovation Project of universities (No.2022KTSCX100); Yiwen Talent Project; Academician He Lin New Medical Research Foundation (No.2021HLKY02).

## Acknowledgments

We would like to thank Editage ([www.editage.cn](http://www.editage.cn)) for English language editing.

## Conflict of interest

The authors declare that the research was conducted in the absence of any commercial or financial relationships that could be construed as a potential conflict of interest.

## Publisher's note

All claims expressed in this article are solely those of the authors and do not necessarily represent those of their affiliated organizations, or those of the publisher, the editors and the reviewers. Any product that may be evaluated in this article, or claim that may be made by its manufacturer, is not guaranteed or endorsed by the publisher.

## Supplementary material

The Supplementary Material for this article can be found online at: <https://www.frontiersin.org/articles/10.3389/fonc.2022.1033044/full#supplementary-material>

**SUPPLEMENTARY FIGURE 1**  
(A-D) Merging of multiple data sets.

**SUPPLEMENTARY FIGURE 2**  
(A-D) grouping cluster analysis plot of dataset. (E-H) sample cluster analysis plot of dataset.

**SUPPLEMENTARY FIGURE 3**  
(A-H) Scalar independence and average connectivity of WGCNA analysis for each dataset.

**SUPPLEMENTARY FIGURE 4**  
(A-H) GSE41328, GSE44076, GSE110223 and GSE110225 datasets were analyzed by MCODE for modular genes merging the top 10 genes of Degree values and removing duplicate values to obtain ferroptosis-related DEGs.

**SUPPLEMENTARY FIGURE 5**  
(A-E) Statistical analysis of immunohistochemistry of key genes. \* $P < 0.05$ , \*\* $P < 0.01$  and \*\*\* $P < 0.001$ .

**SUPPLEMENTARY FIGURE 6**  
The correlation of five core genes in the TIMER database in colon cancer.

## References

- Labianca R, Beretta GD, Kildani B, Milesi L, Merlin F, Mosconi S, et al. Colon cancer. *Crit Rev Oncol/Hematol* (2010) 74:106–33. doi: 10.1016/j.critrevonc.2010.01.010
- Rupnarain C, Dlamini Z, Naicker S, Bhoola K. Colon cancer: genomics and apoptotic events. *Biol Chem* (2004) 385:449–64. doi: 10.1515/BC.2004.053
- Rieger MA, Parlesak A, Pool-Zobel BL, Rechkemmer G, Bode C. A diet high in fat and meat but low in dietary fibre increases the genotoxic potential of 'faecal water'. *Carcinogenesis* (1999) 20:2311–6. doi: 10.1093/carcin/20.12.2311
- Berlau J, Gleit M, Pool-Zobel BL. Colon cancer risk factors from nutrition. *Anal Bioanal Chem* (2004) 378:737–43. doi: 10.1007/s00216-003-2284-4
- Mlecnik B, Bindea G, Kirilovsky A, Angell HK, Obenauf AC, Tosolini M, et al. The tumor microenvironment and immunoscore are critical determinants of dissemination to distant metastasis. *Sci Transl Med* (2016) 8:327ra26. doi: 10.1126/scitranslmed.aad6352
- Galon J, Costes A, Sanchez-Cabo F, Kirilovsky A, Mlecnik B, Lagorce-Pages C, et al. Type, density, and location of immune cells within human colorectal tumors predict clinical outcome. *Science* (2006) 313:1960–4. doi: 10.1126/science.1129139
- Chen H, Luo J, Guo J. Development and validation of a five-immune gene prognostic risk model in colon cancer. *BMC Cancer* (2020) 20:395. doi: 10.1186/s12885-020-06799-0
- Benson AB, Venook AP, Al-Hawary MM, Cederquist L, Chen YJ, Ciombor KK, et al. NCCN guidelines insights: Colon cancer, version 2. *2018 J Natl Compr Canc Netw* (2018) 16:359–69. doi: 10.6004/jnccn.2018.0021
- Dixon SJ, Lemberg KM, Lamprecht MR, Skouta R, Zaitsev EM, Gleason CE, et al. Ferroptosis: an iron-dependent form of nonapoptotic cell death. *Cell* (2012) 149:1060–72. doi: 10.1016/j.cell.2012.03.042
- Fang X, Wang H, Han D, Xie E, Yang X, Wei J, et al. Ferroptosis as a target for protection against cardiomyopathy. *Proc Natl Acad Sci U.S.A.* (2019) 116:2672–80. doi: 10.1073/pnas.1821022116
- Friedmann Angeli JP, Krysko DV, Conrad M. Ferroptosis at the crossroads of cancer-acquired drug resistance and immune evasion. *Nat Rev Cancer* (2019) 19:405–14. doi: 10.1038/s41568-019-0149-1
- Elgendy SM, Alyammahi SK, Alhamad DW, Abdin SM, Omar HA. Ferroptosis: An emerging approach for targeting cancer stem cells and drug resistance. *Crit Rev Oncol Hematol* (2020) 155:103095. doi: 10.1016/j.critrevonc.2020.103095
- Chiappelli F, Balenton N, Khakshooy A. Future innovations in viral immune surveillance: A novel place for bioinformatics and artificial intelligence in the administration of health care. *Bioinformatics* (2018) 14:201–5. doi: 10.6026/97320630014201
- Cao F, Wang C, Long D, Deng Y, Mao K, Zhong H. Network-based integrated analysis of transcriptomic studies in dissecting gene signatures for LPS-induced acute lung injury. *Inflammation* (2021) 44:2486–98. doi: 10.1007/s10753-021-01518-8
- Du S, Zeng F, Sun H, Liu Y, Han P, Zhang B, et al. Prognostic and therapeutic significance of a novel ferroptosis related signature in colorectal cancer patients. *Bioengineered* (2022) 13:2498–512. doi: 10.1080/21655979.2021.2017627
- Zhou N, Bao J. FerrDB: a manually curated resource for regulators and markers of ferroptosis and ferroptosis-disease associations. *Database (Oxford)* 2020(2020):baaa021.8. doi: 10.1093/database/baaa021
- Zhou Y, Zhou B, Pache L, Chang M, Khodabakhshi AH, Tanasechuk O, et al. Metascape provides a biologist-oriented resource for the analysis of systems-level datasets. *Nat Commun* (2019) 10:1523. doi: 10.1038/s41467-019-09234-6
- Liao Y, Wang J, Jaehnic EJ, Shi Z, Zhang B. WebGestalt 2019: gene set analysis toolkit with revamped UIs and APIs. *Nucleic Acids Res* (2019) 47:W199–205. doi: 10.1093/nar/gkz401
- Szklarczyk D, Gable AL, Nastou KC, Lyon D, Kirsch R, Pyysalo S, et al. The STRING database in 2021: customizable protein-protein networks, and functional characterization of user-uploaded gene/measurement sets. *Nucleic Acids Res* (2021) 49:D605–12. doi: 10.1093/nar/gkaa1074
- Cao F, Fan Y, Yu Y, Yang G, Zhong H. Dissecting prognosis modules and biomarkers in glioblastoma based on weighted gene Co-expression network analysis. *Cancer Manag Res* (2021) 13:5477–89. doi: 10.2147/CMAR.S310346
- Xu S, Feng Y, Zhao S. Proteins with evolutionarily hypervariable domains are associated with immune response and better survival of basal-like breast cancer patients. *Comput Struct Biotechnol J* (2019) 17:430–40. doi: 10.1016/j.csbj.2019.03.008
- Shen W, Song Z, Zhong X, Huang M, Shen D, Gao P, et al. Sangerbox: A comprehensive, interaction-friendly clinical bioinformatics analysis platform. *iMeta* (2022) 1:e36. doi: 10.1002/imt2.36
- Vasaikar SV, Straub P, Wang J, Zhang B. LinkedOmics: analyzing multi-omics data within and across 32 cancer types. *Nucleic Acids Res* (2018) 46:D956–63. doi: 10.1093/nar/gkx1090
- Li T, Fan J, Wang B, Traugh N, Chen Q, Liu JS, et al. TIMER: A web server for comprehensive analysis of tumor-infiltrating immune cells. *Cancer Res* (2017) 77:e108–10. doi: 10.1158/1538-7445.AM2017-108
- Zeng D, Ye Z, Shen R, Yu G, Wu J, Xiong Y, et al. IOBR: Multi-omics immuno-oncology biological research to decode tumor microenvironment and signatures. *Front Immunol* (2021) 12:687975. doi: 10.3389/fimmu.2021.687975
- Su Y, Wang J, Quan M. Novel insights into the molecular mechanisms underlying the beneficial effects of exercise training on pulmonary arterial hypertension. *J Sports Med Phys Fitness* (2019) 59:1584–92. doi: 10.23736/S0022-4707.18.09204-6
- Wang W, Green M, Choi JE, Gijon M, Kennedy PD, Johnson JK, et al. CD8(+) T cells regulate tumour ferroptosis during cancer immunotherapy. *Nature* (2019) 569:270–4. doi: 10.1038/s41586-019-1170-y
- Saleh R, Sasidharan Nair V, Toor SM, Taha RZ, Murshed K, Al-Dhaheri M, et al. Differential gene expression of tumor-infiltrating CD8(+) T cells in advanced versus early-stage colorectal cancer and identification of a gene signature of poor prognosis. *J Immunother Cancer* (2020) 8(9–11):e001294. doi: 10.1136/jitc-2020-001294
- Ferlay J, Soerjomataram I, Dikshit R, Eser S, Mathers C, Rebelo M, et al. Cancer incidence and mortality worldwide: sources, methods and major patterns in GLOBOCAN 2012. *Int J Cancer* (2015) 136:E359–86. doi: 10.1002/ijc.29210
- Xie Y, Hou W, Song X, Yu Y, Huang J, Sun X, et al. Ferroptosis: process and function. *Cell Death Differ* (2016) 23:369–79. doi: 10.1038/cdd.2015.158
- Jomova K, Valko M. Advances in metal-induced oxidative stress and human disease. *Toxicology* (2011) 283:65–87. doi: 10.1016/j.tox.2011.03.001
- Gleason A, Bush AI. Iron and ferroptosis as therapeutic targets in Alzheimer's disease. *Neurotherapeutics* (2021) 18:252–64. doi: 10.1007/s13311-020-00954-y
- Borawski B, Malyszko J. Iron, ferroptosis, and new insights for prevention in acute kidney injury. *Adv Med Sci* (2020) 65:361–70. doi: 10.1016/j.advms.2020.06.004
- Ng SW, Norwitz SG, Taylor HS, Norwitz ER. Endometriosis: The role of iron overload and ferroptosis. *Reprod Sci* (2020) 27:1383–90. doi: 10.1007/s43032-020-00164-z
- Baba Y, Higa JK, Shimada BK, Horiuchi KM, Sahara T, Kobayashi M, et al. Protective effects of the mechanistic target of rapamycin against excess iron and ferroptosis in cardiomyocytes. *Am J Physiol Heart Circ Physiol* (2018) 314:H659–68. doi: 10.1152/ajpheart.00452.2017
- Lin GL, Ting HJ, Tseng TC, Juang V, Lo YL. Modulation of the mRNA-binding protein HuR as a novel reversal mechanism of epirubicin-triggered multidrug resistance in colorectal cancer cells. *PLoS One* (2017) 12:e0185625. doi: 10.1371/journal.pone.0185625
- Lan Y, Xiao X, He Z, Luo Y, Wu C, Li L, et al. Long noncoding RNA OCC-1 suppresses cell growth through destabilizing HuR protein in colorectal cancer. *Nucleic Acids Res* (2018) 46:5809–21. doi: 10.1093/nar/gky214
- Lal S, Cheung EC, Zarei M, Preet R, Chand SN, Mambelli-Lisboa NC, et al. CRISPR knockout of the HuR gene causes a xenograft lethal phenotype. *Mol Cancer Res* (2017) 15:696–707. doi: 10.1158/1541-7786.MCR-16-0361
- Lopez de Silanes I, Lal A, Gorospe M. HuR: post-transcriptional paths to malignancy. *RNA Biol* (2005) 2:11–3. doi: 10.4161/rna.2.1.1552
- de Silanes IL, Fan J, Yang X, Zonderman AB, Potapova O, Pizer ES, et al. Role of the RNA-binding protein HuR in colon carcinogenesis. *Oncogene* (2003) 22:7146–54. doi: 10.1038/sj.onc.1206862
- Denkert C, Koch I, von Keyserlingk N, Noske A, Niesporek S, Dietel M, et al. Expression of the ELAV-like protein HuR in human colon cancer: association with tumor stage and cyclooxygenase-2. *Mod Pathol* (2006) 19:1261–9. doi: 10.1038/modpathol.3800645
- Sui M, Xu D, Zhao W, Lu H, Chen R, Duan Y, et al. CIRBP promotes ferroptosis by interacting with ELAVL1 and activating ferritinophagy during renal ischaemia-reperfusion injury. *J Cell Mol Med* (2021) 10:25(13):6203–16. doi: 10.1111/jcmm.16567
- Wang J, Guo Y, Chu H, Guan Y, Bi J, Wang B. Multiple functions of the RNA-binding protein HuR in cancer progression, treatment responses and prognosis. *Int J Mol Sci* (2013) 14:10015–41. doi: 10.3390/ijms140510015
- Srikantan S, Gorospe M. HuR function in disease. *Front Biosci (Landmark Ed)* (2012) 17:189–205. doi: 10.2741/3921
- Zhang Z, Yao Z, Wang L, Ding H, Shao J, Chen A, et al. Activation of ferritinophagy is required for the RNA-binding protein ELAVL1/HuR to regulate

- ferroptosis in hepatic stellate cells. *Autophagy* (2018) 14:2083–103. doi: 10.1080/15548627.2018.1503146
46. Gunton JE. Hypoxia-inducible factors and diabetes. *J Clin Invest* (2020) 130:5063–73. doi: 10.1172/JCI137556
47. Islam F, Gopalan V, Lu CT, Pillai S, Lam AK. Identification of novel mutations and functional impacts of EPAS1 in colorectal cancer. *Cancer Med* (2021) 10:5557–73. doi: 10.1002/cam4.4116
48. Peng Y, Cui C, He Y, Ouzhuluobu H, Zhang, Yang D, et al. Down-regulation of EPAS1 transcription and genetic adaptation of tibetans to high-altitude hypoxia. *Mol Biol Evol* (2017) 34(4):818–30. doi: 10.1093/molbev/msw280
49. Schonenberger MJ, Krek W, Kovacs WJ. EPAS1/HIF-2 $\alpha$  is a driver of mammalian pentoxophagy. *Autophagy* (2015) 11:967–9. doi: 10.1080/15548627.2015.1045180
50. Talks KL, Turley H, Gatter KC, Maxwell PH, Pugh CW, Ratcliffe PJ, et al. The expression and distribution of the hypoxia-inducible factors HIF-1 $\alpha$  and HIF-2 $\alpha$  in normal human tissues, cancers, and tumor-associated macrophages. *Am J Pathol* (2000) 157:411–21. doi: 10.1016/S0002-9440(10)64554-3
51. Kaidi A, Qualtrough D, Williams AC, Paraskeva C. Direct transcriptional up-regulation of cyclooxygenase-2 by hypoxia-inducible factor (HIF)-1 promotes colorectal tumor cell survival and enhances HIF-1 transcriptional activity during hypoxia. *Cancer Res* (2006) 66:6683–91. doi: 10.1158/0008-5472.CAN-06-0425
52. Mohammed N, Rodriguez M, Garcia V, Garcia JM, Dominguez G, PeÑA C, et al. EPAS1 mRNA in plasma from colorectal cancer patients is associated with poor outcome in advanced stages. *Oncol Lett* (2011) 2:719–24. doi: 10.3892/ol.2011.294
53. Singhal R, Mitta SR, Das NK, Kerk SA, Sajjakulnukit P, Solanki S, et al. HIF-2 $\alpha$  activation potentiates oxidative cell death in colorectal cancers by increasing cellular iron. *J Clin Invest* (2021) 131(12):e143691. doi: 10.1172/JCI143691
54. Zou Y, Palte MJ, Deik AA, Li H, Eaton JK, Wang W, et al. A GPX4-dependent cancer cell state underlies the clear-cell morphology and confers sensitivity to ferroptosis. *Nat Commun* (2019) 10:1617. doi: 10.1038/s41467-019-09277-9
55. Zhou X, Zheng Y, Sun W, Zhang Z, Liu J, Yang W, et al. D-mannose alleviates osteoarthritis progression by inhibiting chondrocyte ferroptosis in a HIF-2 $\alpha$ -dependent manner. *Cell Prolif* (2021) 54:e13134. doi: 10.1111/cpr.13134
56. Chu FF, Esworthy RS, Chu PG, Longmate JA, Huycke MM, Wilczynski S, et al. Bacteria-induced intestinal cancer in mice with disrupted Gpx1 and Gpx2 genes. *Cancer Res* (2004) 64:962–8. doi: 10.1158/0008-5472.CAN-03-2272
57. Ukai Y, Kishimoto T, Ohdate T, Izawa S, Inoue Y. Glutathione peroxidase 2 in *Saccharomyces cerevisiae* is distributed in mitochondria and involved in sporulation. *Biochem Biophys Res Commun* (2011) 411:580–5. doi: 10.1016/j.bbrc.2011.06.189
58. Canizal-Garcia M, Olmos-Orizaba BE, Moreno-Jimenez M, Calderon-Cortes E, Saavedra-Molina A, Cortes-Rojo C. Glutathione peroxidase 2 (Gpx2) preserves mitochondrial function and decreases ROS levels in chronologically aged yeast. *Free Radic Res* (2021) 55:165–75. doi: 10.1080/10715762.2021.1882677
59. Banning A, Deubel S, Kluth D, Zhou Z, Brigelius-Flohé R. The GI-GPx gene is a target for Nrf2. *Mol Cell Biol* (2005) 25:4914–23. doi: 10.1128/MCB.25.12.4914-4923.2005
60. Banning A, Florian S, Deubel S, Thalmann S, Muller-Schmehl K, Jacobasch G, et al. GPx2 counteracts PGE2 production by dampening COX-2 and mPGES-1 expression in human colon cancer cells. *Antioxid Redox Signal* (2008) 10:1491–500. doi: 10.1089/ars.2008.2047
61. Hendrickse CW, Kelly RW, Radley S, Donovan IA, Keighley MR, Neoptolemos JP. Lipid peroxidation and prostaglandins in colorectal cancer. *Br J Surg* (1994) 81:1219–23. doi: 10.1002/bjs.1800810849
62. Emmink BL, Laoukili J, Kipp AP, Koster J, Govaert KM, Fatrai S, et al. GPx2 suppression of H<sub>2</sub>O<sub>2</sub> stress links the formation of differentiated tumor mass to metastatic capacity in colorectal cancer. *Cancer Res* (2014) 74:6717–30. doi: 10.1158/0008-5472.CAN-14-1645
63. Kipp A, Banning A, Brigelius-Flohe R. Activation of the glutathione peroxidase 2 (GPx2) promoter by beta-catenin. *Biol Chem* (2007) 388:1027–33. doi: 10.1515/BC.2007.137
64. Li F, Dai L, Niu J. GPX2 silencing relieves epithelial-mesenchymal transition, invasion, and metastasis in pancreatic cancer by downregulating wnt pathway. *J Cell Physiol* (2020) 235:7780–90. doi: 10.1002/jcp.29391
65. Brigelius-Flohe R, Kipp AP. Physiological functions of GPx2 and its role in inflammation-triggered carcinogenesis. *Ann N Y Acad Sci* (2012) 1259:19–25. doi: 10.1111/j.1749-6632.2012.06574.x
66. Musumeci D, Roviello GN, Montesarchio D. An overview on HMGB1 inhibitors as potential therapeutic agents in HMGB1-related pathologies. *Pharmacol Ther* (2014) 141:347–57. doi: 10.1016/j.pharmthera.2013.11.001
67. Lee H, Shin N, Song M, Kang UB, Yeom J, Lee C, et al. Analysis of nuclear high mobility group box 1 (HMGB1)-binding proteins in colon cancer cells: clustering with proteins involved in secretion and extranuclear function. *J Proteome Res* (2010) 9:4661–70. doi: 10.1021/pr100386r
68. Wang FC, Pei JX, Zhu J, Zhou NJ, Liu DS, Xiong HF, et al. Overexpression of HMGB1 a-box reduced lipopolysaccharide-induced intestinal inflammation via HMGB1/TLR4 signaling in vitro. *World J Gastroenterol* (2015) 21:7764–76. doi: 10.3748/wjg.v21.i25.7764
69. Evankovich J, Cho SW, Zhang R, Cardinal J, Dhupar R, Zhang L, et al. High mobility group box 1 release from hepatocytes during ischemia and reperfusion injury is mediated by decreased histone deacetylase activity. *J Biol Chem* (2010) 285:39888–97. doi: 10.1074/jbc.M110.128348
70. Kuniyasu H, Yano S, Sasaki T, Sasahira T, Sone S, Ohmori H. Colon cancer cell-derived high mobility group 1/Amphotericin induces growth inhibition and apoptosis in macrophages. *Am J Pathol* (2005) 166:751–9. doi: 10.1016/S0002-9440(10)62296-1
71. Wen Q, Liu J, Kang R, Zhou B, Tang D. The release and activity of HMGB1 in ferroptosis. *Biochem Biophys Res Commun* (2019) 510:278–83. doi: 10.1016/j.bbrc.2019.01.090
72. Kang HJ, Lee H, Choi HJ, Youn JH, Shin JS, Ahn YH, et al. Non-histone nuclear factor HMGB1 is phosphorylated and secreted in colon cancers. *Lab Invest* (2009) 89:948–59. doi: 10.1038/labinvest.2009.47
73. Wang Y, Chen Q, Shi C, Jiao F, Gong Z. Mechanism of glycyrrhizin on ferroptosis during acute liver failure by inhibiting oxidative stress. *Mol Med Rep* (2019) 20:4081–90. doi: 10.3892/mmr.2019.10660
74. Ye F, Chai W, Xie M, Yang M, Yu Y, Cao L, et al. HMGB1 regulates erastin-induced ferroptosis via RAS-JNK/p38 signaling in HL-60/NRASQ61L cells. *Am J Cancer Res* (2019) 9(4):730–9.
75. Scanga R, Scalise M, Rovella F, Regina TMR, Galluccio M, Indiveri C. The nutraceutical alliin from garlic is a novel substrate of the essential amino acid transporter LAT1 (SLC7A5). *Front Pharmacol* (2022) 13:877576. doi: 10.3389/fphar.2022.877576
76. Cosco J, Scalise M, Colas C, Galluccio M, Martini R, Rovella F, et al. ATP modulates SLC7A5 (LAT1) synergistically with cholesterol. *Sci Rep* (2020) 10:16738. doi: 10.1038/s41598-020-73757-y
77. Cormerais Y, Massard PA, Vucetic M, Giuliano S, Tambutte E, Durivault J, et al. The glutamine transporter ASCT2 (SLC1A5) promotes tumor growth independently of the amino acid transporter LAT1 (SLC7A5). *J Biol Chem* (2018) 293:2877–87. doi: 10.1074/jbc.RA117.001342
78. Kaira K, Oriuchi N, Imai H, Shimizu K, Yanagitani N, Sunaga N, et al. Prognostic significance of l-type amino acid transporter 1 expression in resectable stage I-III nonsmall cell lung cancer. *Br J Cancer* (2008) 98:742–8. doi: 10.1038/sj.bjcr.6604235
79. Ishimoto T, Nagano O, Yae T, Tamada M, Motohara T, Oshima H, et al. CD44 variant regulates redox status in cancer cells by stabilizing the xCT subunit of system xc(-) and thereby promotes tumor growth. *Cancer Cell* (2011) 19:387–400. doi: 10.1016/j.ccr.2011.01.038